Supplementary Material

Fieldwork, geomorphic setting and stratigraphy

Supplementary Figure 1. Satellite imagery supplied by Google Earth illustrating the location within southeastern Australia of the sampling sites. The insets show the Willandra Lakes sites Ram Paddock and Well Paddock relative to lakes Mungo and Durthong; and the Spring Creek site relative to Mount Rouse.

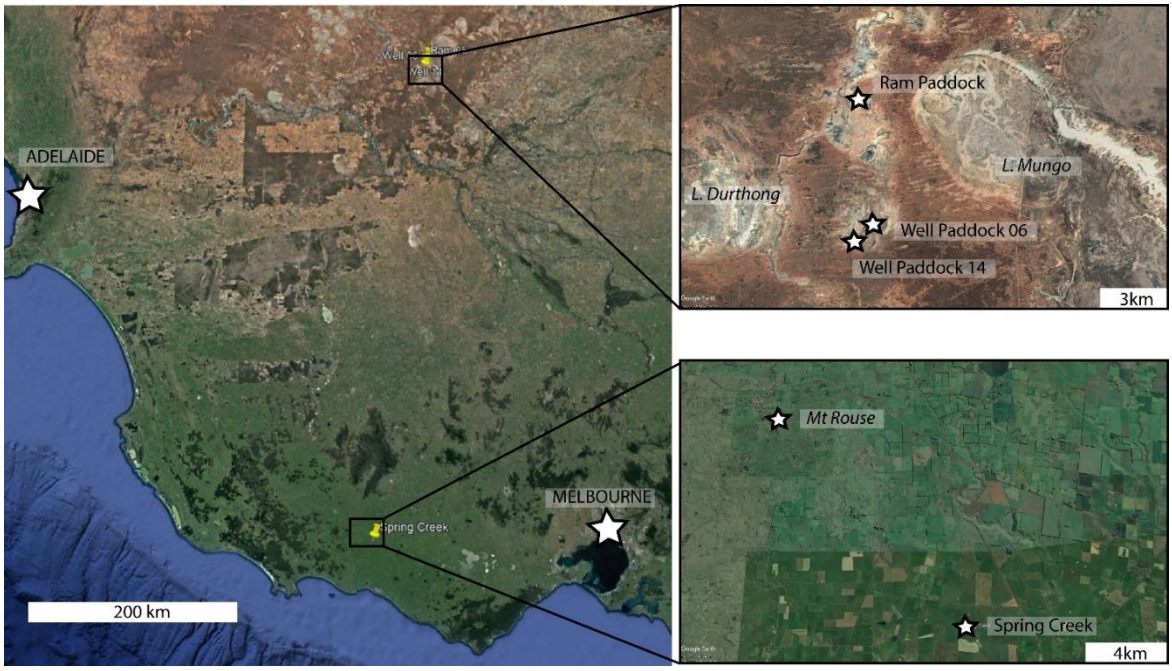

Supplementary Figure 2. Photograph of the vicinity of the Well Paddock 06 sampling site (looking south), showing the alternating clayey and sandy sediments of the innermost lunette at Well Paddock Lake.

OSL sampling at Spring Creek was undertaken at Section A (Figure S3), downstream of the main bone bed but interpreted as its stratigraphic equivalent (Porch and Kershaw 2010). The initial aim was to constrain the timing of deposition of the dark laminated clayey silts associated with both the megafauna and fossil beetle assemblage, independently of the radiocarbon dating from this and the adjacent setting. Three samples were collected from the dark laminated clayey silts immediately overlying the Tertiary marls, and underlying a thin lamina of ferruginous gravel representing the upper unit of ferruginous sandy silts (Figure S3, Table S3). Samples were collected by driving 4 cm diameter, 10 cm long stainless-steel tubes horizontally into the cleaned section. These holes were then widened and deepened by hand auger to accommodate a portable sodium iodide gamma spectrometer with a three-inch crystal detector; gamma spectra were measured within each hole for half an hour.

Supplementary Figure 3. Stratigraphy and sampling at the Spring Creek locality. Sections A-C show the primary stratigraphic sequence and correlations, from several metres below the waterfall (C) to the head of the downstream pool (A). The dark, clayey silts of section A are laminated in comparison to those in sections B and C, which are more massive in character. Samples for pollen and beetle analysis, radiocarbon and OSL dating were collected from the laminated sediments at section A. Additional pollen, beetle and radiocarbon samples were collected from section B. The beetle/radiocarbon samples at section B were collected from the intersection between the basal bone bed and overlying clayey silts.

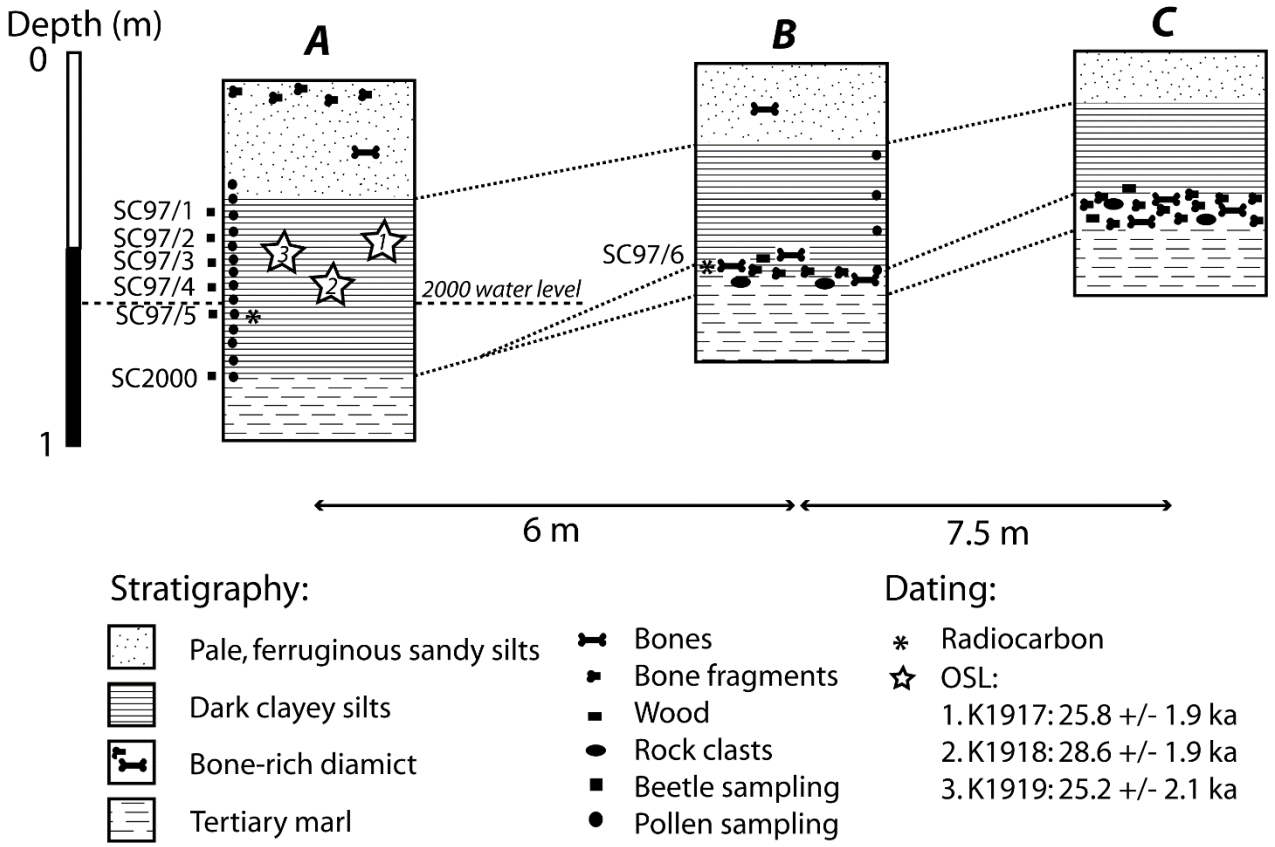

Supplementary Table 1. Description and setting of the Ram Paddock Lake sampling site.

Locality	Coordinates	Elevation	Setting	Stratigraphy	Age (ka)
RAM05	33°38.738'S 142°56.449'E	72 m ASL	Low angle, low altitude pelletal clay source-bordering dune	Reddish-brown, compact sandy clays with minor coarse sand. Overlain by post-European unconsolidated brown sands with fencing wire	22.7 ± 1.8

Supplementary Table 2. Description and setting of the Well Paddock Lake sampling sites.

Locality	Coordinates	Elevation	Setting	Stratigraphy	Age (ka)
WELL03	33°42.128'S 142°56.065'E		Southwest lake shoreline with substantial gullying	Underlying grey-greenish lake clays with strong carbonate-rich soil development, overlain by orange-brown sands (alluvial?) and aeolian sands	Not sampled due to bioturbation by grazing animals
WELL06	33°42.143'S 142°56.261'E	65 m ASL	Inner (final phase) lunette; small blowout facing NW and close to lunette crest	Upper unit: pale yellowish brown, well sorted fine to medium aeolian sands with weak soil polygon development. Lower unit: pale brown pelletal clay dune with minor coarse-	21.1 ± 1.8 (upper unit) 19.1 ± 1.5 (lower unit)

				grained quartz sand	
WELL14	33°41.772'S 142°56.799'E	71 m ASL	Just below crest of outer lunette	Alternating sands and clayey sands (indicating oscillating lake levels), some pedogenesis. Equivalent to Upper Mungo (weighted mean age 36.6 ± 4.6 ka; (Fitzsimmons et al. 2015)?	29.0 ± 2.2

Supplementary Table 3. Combined stratigraphy of the Spring Creek site (profiles A, B and C). Ages associated with the respective units are listed (OSL ages in plain text, calibrated radiocarbon dates in italics).

Depth range (m)	**Description – sections**			**Ages (ka/ *ky cal BP*)**
	A	**B**	**C**	
0.00 – 0.30 (A) 0.00 – 0.20 (B) 0.00 – 0.10 (C)	Pale, ferruginous sandy silts with sparse bone fragments; ferruginous gravels at base of unit; bone fragments increase in frequency towards the surface	Pale, ferruginous sandy silts with sparse bone fragments	Pale, ferruginous sandy silts	<25 (estimate based on OSL ages)
0.30 – 0.85 (A) 0.20 – 0.50 (B) 0.10 – 0.30 (C)	Laminated grey, clayey silts with high organic content	Massive grey, clayey silts	Massive grey, clayey silts	<u>Section A:</u> 25.8 ± 2.0 25.2 ± 2.3 28.7 ± 2.1

0.85 – 0.90 (A) 0.45 – 0.55 (B) 0.30 – 0.45 (C)	Laminated, organic grey silts with sparse wood and bone fragments	Bone-rich diamict, including basalt rock and wood fragments. Grades into massive grey silts of overlying unit	Bone-rich diamict, including basalt rock and wood fragments	*<u>Section A:</u>* *>46639* *>44399* *41927* *<u>Section B:</u>* *>45347* *>43769* *41924 ± 2039* *45809 ± 4764*
>0.90 (A) >0.55 (B) >0.45 (C)	Tertiary marls	Tertiary marls	Tertiary marls	Tertiary

Luminescence dating

The Spring Creek samples were processed in the laboratory under low intensity red light and sodium vapour lamps. Sediment from the central section of the tubes was processed for dating. Samples were treated by digestion in dilute hydrochloric acid (HCl) and hydrogen peroxide, followed by sieving to isolate the 125-180 µm sand size fraction, density separation using sodium polytungstate solution prepared to 2.68 $g.cm^{-3}$, and etching in 40% solution of hydrofluoric acid for 100 minutes, with a final rinse in HCl and sieving to remove small quartz flakes produced as a result of etching. The resulting clean quartz grains were then prepared as aliquots mounted onto the central 3 mm of 10 mm diameter stainless steel discs using silicone oil. 24 aliquots were prepared for samples K1917 and K1918, and 12 aliquots from K1919 due to the limited amount of quartz recovered from this sample.

Equivalent dose (D_e) measurements were undertaken using automated Risø TL-DA-15 and TL-DA-12 readers equipped with blue light-emitting diodes for light stimulation (Botter-Jensen et al. 2000; Botter-Jensen, Mejdahl, and Murray 1999). Irradiation was provided by calibrated $^{90}Sr/^{90}Y$ beta sources(Botter-Jensen et al. 2000). Luminescence signals were detected by EMI 9235QA photomultiplier tubes with coated Hoya U-340 filters (Botter-Jensen 1997). The D_e was measured using the single-aliquot regenerative-dose (SAR) protocol of Murray and Wintle (2000; 2003), incorporating an infrared-stimulated luminescence (IRSL) was prior to each OSL measurement to identify potential feldspar contamination of the samples (Murray and Wintle 2003). Preheat and cutheat temperatures of 260ºC and 220ºC respectively were determined based on the results of preheat plateau tests on samples from nearby sites in southeastern Australia, which showed no dependence of dose on temperature (Fitzsimmons, Rhodes, and Barrows 2010). The resulting dose values yielded normal distributions (Figure_OSL a-c); consequently, the Central Age Model (CAM) of Galbraith et al. (1999) was used for age calculation.

The beta component of the environmental radiation dose rate was calculated using the concentrations of radioactive isotopes U, Th and K present in the sediments, and the conversion factors of Adamiec and Aitken (1998). These were analysed using inductively-coupled plasma (ICP) mass spectrometry

for U and Th, and ICP atomic emission spectrometry for K, at Genalysis Laboratories, Perth, Western Australia. The water content of the samples was assumed to represent the long-term and spatial average, and was incorporated into the dose rate calculations to correct for the attenuation of radiation by moisture (Mejdahl 1979). Since the samples were collected close to the present-day water level, moisture content was comparable with saturation. Material from the ends of the sample tubes was used to calculate in-situ moisture content by weighing the natural and oven-dried weight; this was averaged for the three samples. A value of 28 ± 10% was therefore used for all samples. The gamma component of the sample dose rates was calculated using in situ gamma spectrometry, and the cosmic ray component of the dose rate was calculated based on equations published in Prescott and Hutton (1994).

The Spring Creek sediments are not rich in sand-sized quartz, since the sampled unit comprises mostly clayey silts, however the material which was recovered for OSL measurement appear to be well suited to luminescence dating. All samples exhibit bright, rapidly decaying signals typical of strongly sensitive quartz dominated by the fast component (Figure S6). All aliquots yield dose response characteristics corresponding to an exponential function (Figure S6), suggesting first order kinetics deriving from the fast component trap within the quartz. IRSL signals and thermal transfer of charge are both negligible, and recycling ratios all lie within one standard deviation of unity. The majority of aliquots exhibit minimal change in sensitivity following successive regenerative doses (Figure S6). Normalised sensitivity ratios lie within 50% of that derived from the initial test dose, although a general increase can be observed. Each of the three samples yield normal distributions with one or two outliers (Figure S6). This suggests that the sediments were generally well bleached with respect to the OSL signal at deposition. Overdispersion ranges between 18-23%. These characteristics combined suggest that the quartz sand samples from Spring Creek are highly suitable for OSL dating using the SAR protocol.

All three of the Spring Creek age estimates lie within 2σ error of one another, and the two uppermost samples – K1917 and K1919 – lie within 1σ error. The results suggest that the sediment comprising this stratigraphic unit was deposited relatively rapidly, most likely over a period of several thousand years, around ~29-25 ka. This period corresponds to the later part of marine isotope stage (MIS) 3, and the lead-in to the last glacial maximum (LGM). The OSL dating contrast with those from the AMS radiocarbon analyses (Table 1; Porch and Kershaw 2010). These yield substantially older dates, including two samples from Section A which indicate deposition beyond radiocarbon dating limits.

Supplementary Figure 4. Luminescence characteristics of the sample EVA1125 from Ram Paddock Lake. (A) Radial plot showing the dose distributions, indicating the equivalent dose populations identified during the finite mixture modelling; the final D_e used for age calculation is given by the horizontal shading which corresponds to its 2σ range. (B) Natural OSL decay curve for a representative grain and showing the integration limits used for calculation of the grain dose. (C) Dose-response curve for the same grain shown in (B). (D) Test-dose sensitivity change across regenerative cycles of the single aliquot regenerative dose (SAR) protocol, normalized to the first test-dose response (T_n) obtained after measurement of the natural signal.

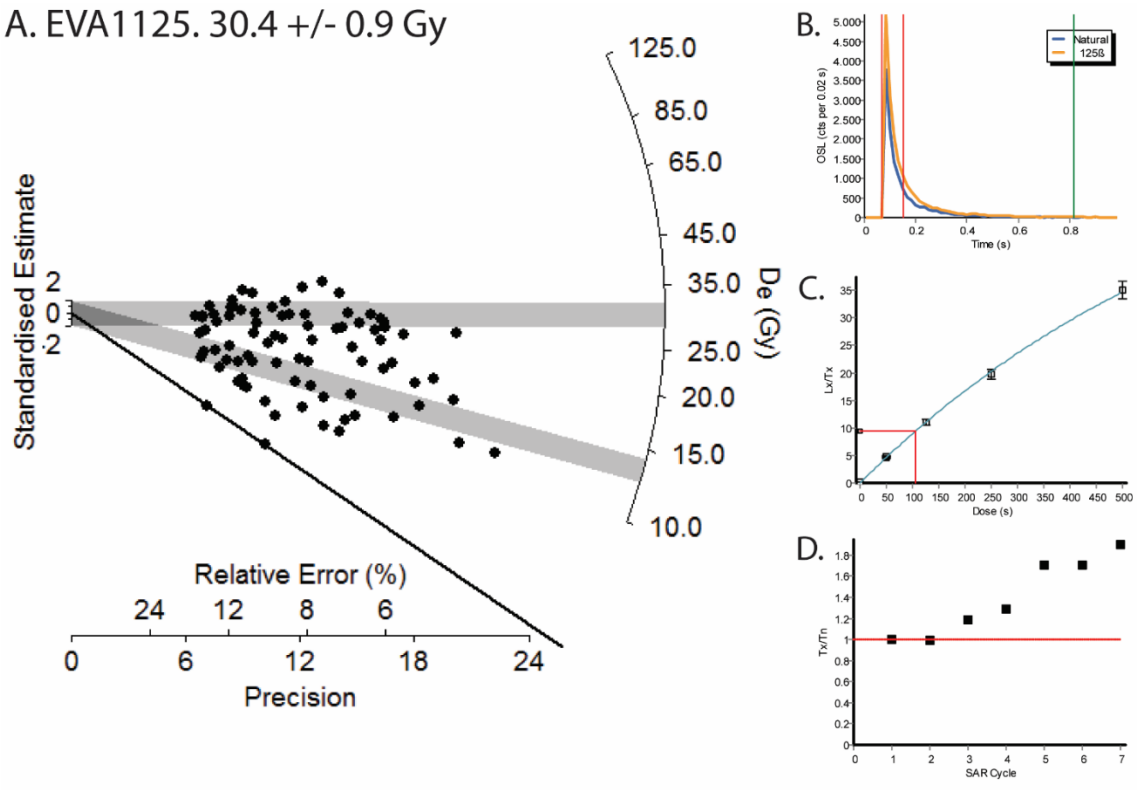

Supplementary Figure 5. Luminescence characteristics of the samples from Well Paddock Lake: (A) EVA1126, (B) EVA1127 and (C) EVA1128. The respective main plots on the left-hand side are radial plots showing the dose distributions; for (A) EVA1126 we show the three equivalent dose populations identified during the finite mixture modelling (the final D_e used for age calculation is given by horizontal shading which corresponds to the 2σ range). On the right are shown respectively, for representative grains of each sample, the natural OSL decay curves, dose-response curves and test-dose sensitivity change across regenerative cycles of the single aliquot regenerative dose (SAR) protocol, normalized to the first test-dose response (T_n) obtained after measurement of the natural signal.

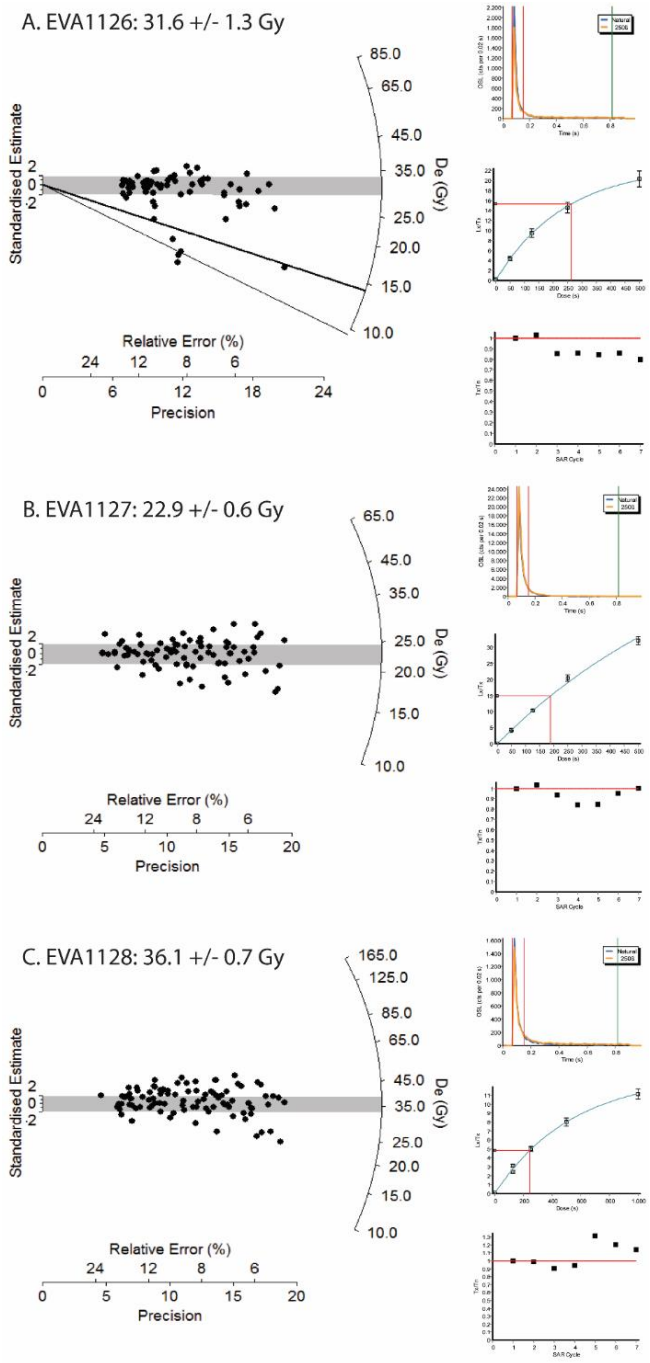

Supplementary Figure 6. Luminescence characteristics of the Spring Creek sediments: Radial plots showing dose distributions for K1917 (A), K1918 (B) and K1919 (C). The shaded area corresponds to 2σ from the equivalent dose (D_e), calculated using the Central Age Model of Galbraith et al. (1999). The radial plots illustrate the distributions of ages for each aliquot (right-hand radial y-axis) relative to precision (x-axis). Insets to (A) show the natural OSL decay curve (upper) and dose-response curve (lower) for a typical small aliquot of sample K1917. (D) Test-dose sensitivity change across regenerative cycles of the single aliquot regenerative dose (SAR) protocol, normalized to the first test-dose response (T_n) obtained after measurement of the natural signal, for 12 aliquots of sample K1917.

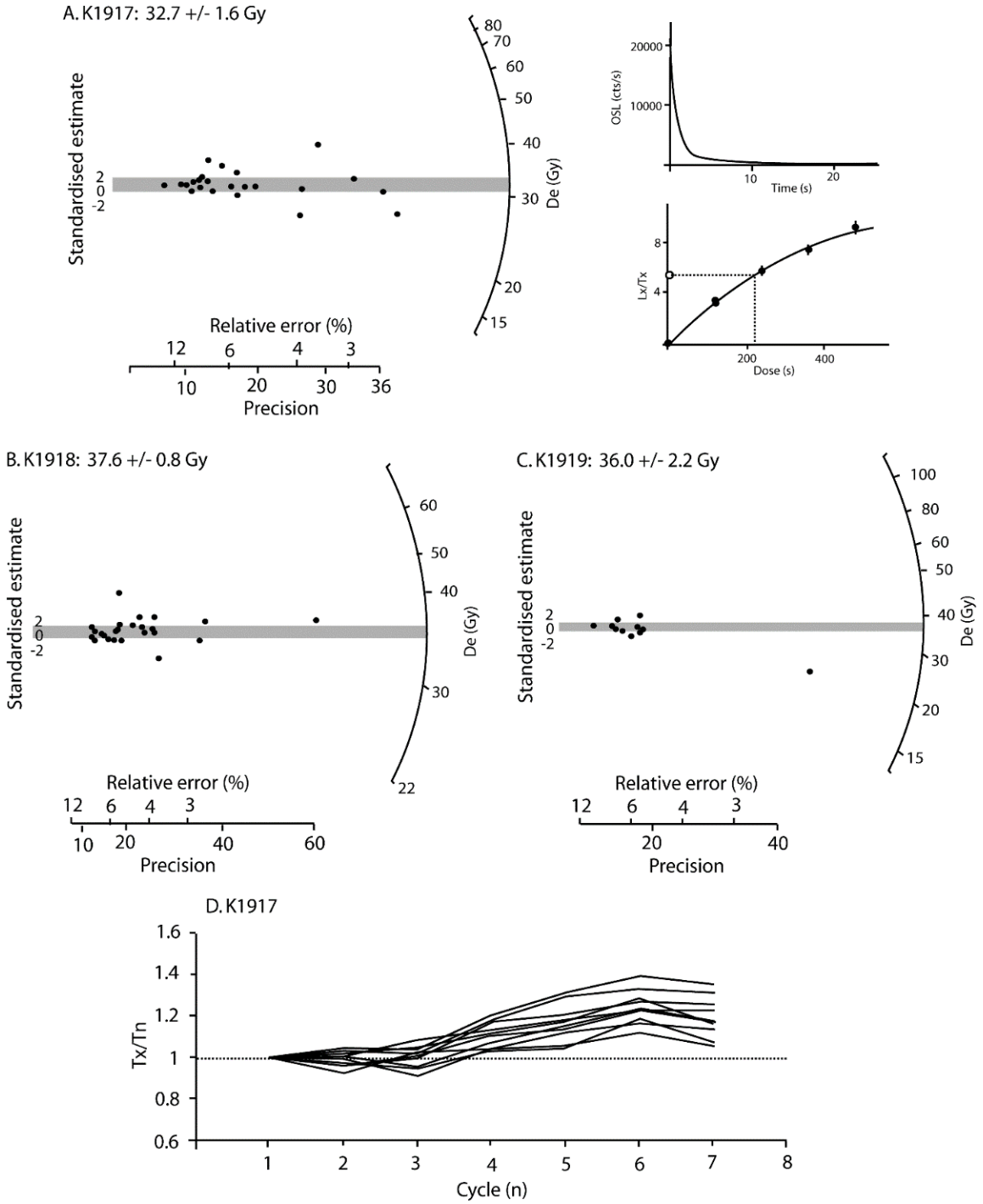

Supplementary Table 4. Summary of luminescence statistics for all samples, including grain/aliquot acceptance rate, recycling ratio, recuperation and overdispersion.

Sample code	**Grains/aliquots accepted (measured)**	**Recycling ratio**	**Recuperation**	**Overdispersion (%)**
Willandra Lakes (single grains)				
EVA1125	85 (600)	1.00 ± 0.10	0.99 ± 0.19	15.6
EVA1126	63 (600)	0.99 ± 0.08	0.83 ± 0.12	35.3
EVA1127	87 (600)	1.00 ± 0.10	1.1 ± 0.2	20.2
EVA1128	147 (600)	0.99 ± 0.07	1.2 ± 0.2	23.3
Spring Creek (single aliquots)				
K1917	24 (24)	0.99 ± 0.06	0.6 ± 0.3	23.7
K1918	24 (24)	0.99 ± 0.06	1.3 ± 1.5	18.0
K1919	12 (12)	0.99 ± 0.06	1.1 ± 1.1	19.8

Supplementary Table 5. Luminescence dating data for the Willandra Lakes samples.

Laboratory code	EVA1125	EVA1126	EVA1127	EVA1128
Age model	FMM	CAM	CAM	CAM
De (Gy)	30.4	31.6	22.9	36.1
uncertainty	0.9	1.3	0.55	0.7
Overdispersion (%)	15.6	35.3	20.2	23.3
Measured concentrations				
% K	0.62	0.81	0.45	0.70
error (%K)	0.08	0.08	0.08	0.08
Th (ppm)	5.11	5.93	3.76	3.79
error (ppm)	0.22	0.25	0.15	0.19
U (ppm)	1.03	1.29	1.04	0.80
error (ppm)	0.15	0.11	0.10	0.09
Beta counter	0.89	1.13	0.69	0.84
Attenuated beta	0.75	0.95	0.58	0.71
External gamma (Gy/ka)	0.51	0.62	0.41	0.44
error	0.05	0.06	0.04	0.04
Cosmic dose calculations				
Depth (m)	0.85	0.40	0.30	0.35
error (m)	0.05	0.05	0.05	0.05
Average overburden density (g.cm^3)	1.90	1.90	1.90	1.90
error (g.cm^3)	0.10	0.10	0.10	0.10
Latitude (deg.)	-34	-34	-34	-34
Longditude (deg.)	143	143	143	143
Altitude (m asl))	72	65	65	71
Cosmic dose rate (Gy/ka)	0.15	0.15	0.16	0.16
Error	0.01	0.02	0.03	0.03
Moisture content				
Moisture (water / wet sediment)	0.05	0.05	0.05	0.05
error	0.03	0.03	0.03	0.03
Total dose rate, Gy/ka	1.34	1.65	1.09	1.24
error	0.10	0.11	0.09	0.09
% error	7.3	6.4	8.0	7.3
AGE (ka)	22.7	19.1	21.1	29.0
error	1.8	1.5	1.8	2.2
% error	7.9	7.6	8.4	7.5

Supplementary Table 6. Luminescence dating data for the Spring Creek samples.

Laboratory code	K1917	K1918	K1919
Age model	CAM	CAM	CAM
De (Gy)	32.7	36.2	26.0
uncertainty	1.7	1.6	2.3
Overdispersion (%)	23.7	18.0	19.8
Measured concentrations			
% K	0.46	0.47	0.36
error (%K)	0.01	0.01	0.01
Th (ppm)	8.95	8.24	12.26
error (ppm)	0.16	0.16	0.16
U (ppm)	1.28	1.21	2.91
error (ppm)	0.16	0.16	0.16
Attenuated beta	0.66	0.63	0.79
External gamma (Gy/ka)	0.557	0.583	0.594
error	0.004	0.004	0.004
Cosmic dose calculations			
Depth (m)	0.20	0.31	0.27
error (m)	0.02	0.02	0.02
Average overburden density (g.cm^3)	1.90	1.90	1.90
error (g.cm^3)	0.10	0.10	0.10
Latitude (deg.)	-38	-38	-38
Longditude (deg.)	142	142	142
Altitude (m asl))	150	150	150
Cosmic dose rate (Gy/ka)	0.12	0.12	0.12
error	0.01	0.01	0.01
Moisture content			
Moisture (water / wet sediment)	0.28	0.28	0.28
error	0.10	0.10	0.10
Total dose rate, Gy/ka	1.27	1.26	1.43
error	0.07	0.07	0.09
% error	5.9	5.8	6.5
AGE (ka)	25.8	28.7	25.2
error	2.0	2.1	2.3
% error	7.9	7.2	9.1

Supplementary Table 7. Summary of finite mixture modelling populations for the relevant single grain dated samples from Ram and Well Paddock Lakes, Willandra. The final accepted equivalent doses are highlighted using italics. In the case of sample EVA1125, the older population was selected for final age analysis since it has the lowest overdispersion of the major populations identified. The oldest population was selected for sample EVA1126 since it corresponds to the majority population of grains.

Sample	**Number of components**	**D_e (Gy)**	**Overdispersion (%)**	**% of grain population**
EVA1125	3	13.5 ± 0.6 4.1 ± 0.3 *30.4 ± 0.9*	30.9 0 15.6	54 2 44
EVA1126	3	9.0 ± 0.3 13.9 ± 0.6 *27.7 ± 1.3*	0 0 35.3	6 3 91

Comments on the megafaunal dating conundrum at Spring Creek

Spring Creek was initially argued to be the site of late survival of several extinct megafaunal species, based on conventional radiocarbon dating of plant remains associated with the bone bed (19800 +/- 390 uncal kBP; Flannery and Gott, 1984). Subsequent AMS radiocarbon measurements directly applied to bone material yielded substantially older dates (27268 ± 330 BP, 27863 ± 333 BP for *Macropus giganteus* bones; 36500 ± 2400 BP, 25440 ± 150 BP on two halves of a single *Palorchestes* humerus), and led to the interpretation that the bone samples were most likely subject to contamination of younger organic material, and could not reliably be dated (White and Flannery 1995). Despite divided speculation as to the nature of deposition of the bone bed, its depositional context remained undated. The antiquity of the fossil remains could likewise not be determined directly, although there was agreement that the site was most likely older than 35 ka (White and Flannery 1995). More recent AMS radiocarbon dating of plant and invertebrate material associated with the bone bed yielded background dates (Table 2; Porch and Kershaw 2010) indicating that the megafaunal remains predated 43 ky BP, in alignment with the model for megafaunal extinction around 46.4 ± 4.8 ka (Roberts et al., 2001).

Our study dates the deposition of the clayey silt sediments believed to be associated with the bone bed. Our results yield substantially younger age estimates for the deposition of the clayey silt sediments believed to be associated with the bone bed. Since the OSL ages appear to reflect well bleached sediment deposited rapidly between ~29-25 ka, it is necessary to revisit the proposed mechanisms for sediment deposition at the site.

We obtained substantially younger age estimates than the underlying organic material, and substantially younger ages than were obtained from the seed and beetle remains contained within the unit (Table 1). Since our OSL ages indicate well bleached sediment deposited rapidly c. 29-25 ka, we must reassess the proposed mechanisms for sediment deposition at the site. The excavated fossil assemblage yielded articulated yet consistently weathered bones (Flannery and Gott 1984; White and Flannery 1995). The density of bone preservation is greater above a small waterfall just upstream of the sampled profile (Porch and Kershaw 2010), suggesting redeposition of megafaunal material subsequent to death and initial deposition on the bone bed. The fossil seed and beetle remains were

sampled at different depths within the clayey silts and yield infinite or minimum dates (Porch and Kershaw, 2010), implying that they were, like the megafauna, redeposited downstream after death. The OSL signal of the sediments, by contrast, would have been reset at the time of sediment deposition. Even though the OSL samples were collected stratigraphically higher than the bulk of the megafaunal deposit, we propose that fossil material collected upstream on the creek bed prior to c. 42 ka and was redeposited a short distance downstream c. 29-25 ka (the timing of sediment deposition) under a relatively low energy environment which preserved the integrity of the organic remains.

Wind regime statistics

The following figures show wind regime/precipitation statistics derived for the observed present day and simulated LGM conditions at the Willandra Lakes and Spring Creek sites. Shaded area presents the wind direction-strength occurrence histogram (percent total scale). Sector line plots show wind speed (black), wind occurrence (red solid), precipitation rate (blue dashed) and total precipitation (red dashed, normalised) distribution about rhumbs. Thin solid/long-dashed line circles indicate the scalar/absolute winds strength and direction, respectively; thin-dashed circle approximates wind vector standard deviation (SD). Wind direction is meteorological (i.e., from where wind blows). Further statistics tabled: V_S and V_R − absolute and scalar wind speed [m/s], R_w and R_p − rhumbs of maximum wind and precipitation occurrence [percent], Q − wind steadiness (V_S/V_R ratio), r_{xy} − wind zonal and meridional components correlation, σ_r − wind vector SD [m/s], λ − wind absolute speed to SD ratio, $\Sigma(P)$ – average total annual/seasonal precipitation [mm].

Figures panels present (A) Annual overall and seasonal statistics for (B) Autumn (March, April, May), (C) Winter (June, July, August), (D) Spring (September, October, November) and (E) Summer (December, January, February), respectively.

Supplementary Figure 7. Wind regime statistics for the present day at the Willandra Lakes.

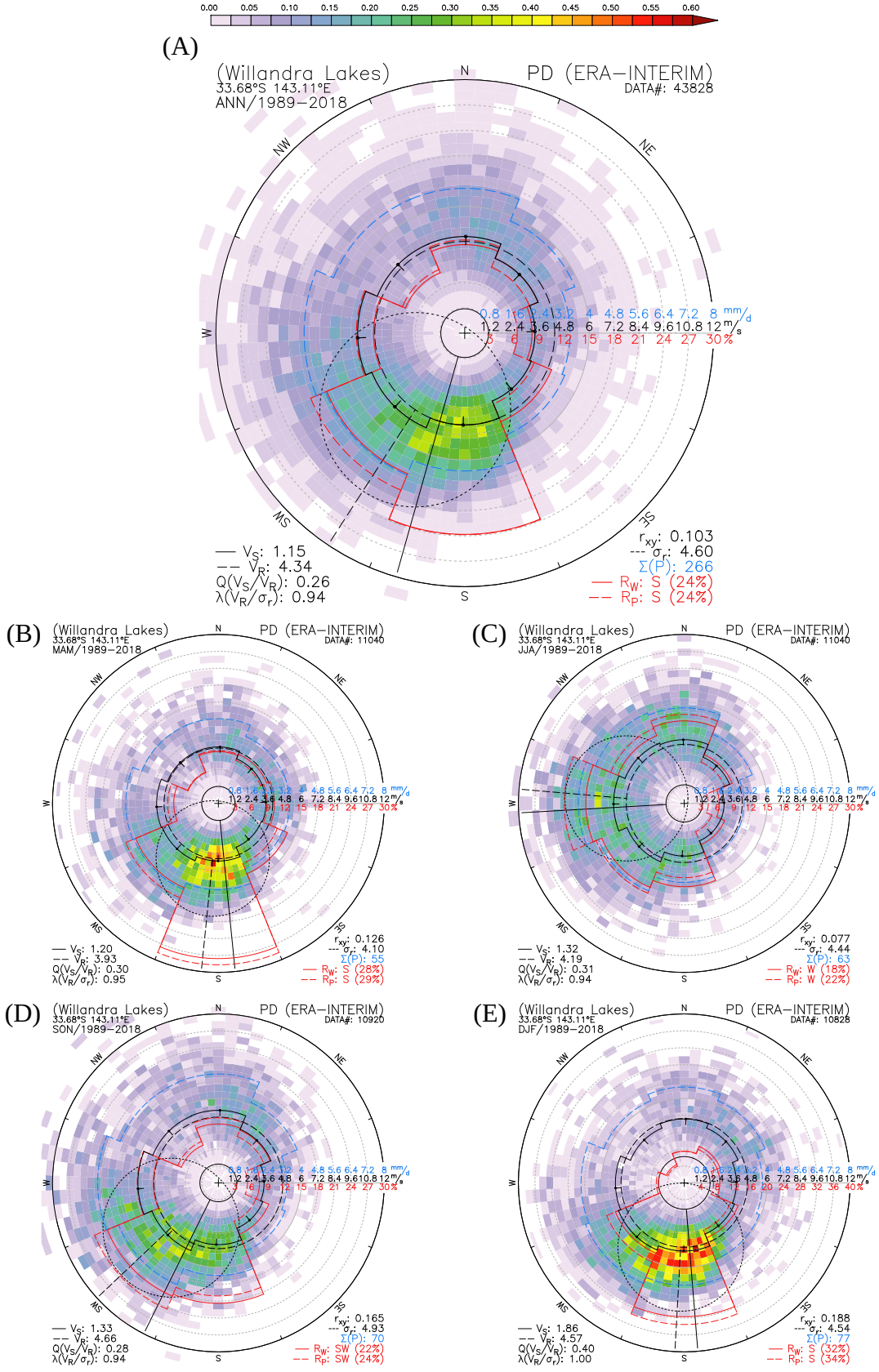

Supplementary Figure 8. Wind regime statistics for the present day at Spring Creek.

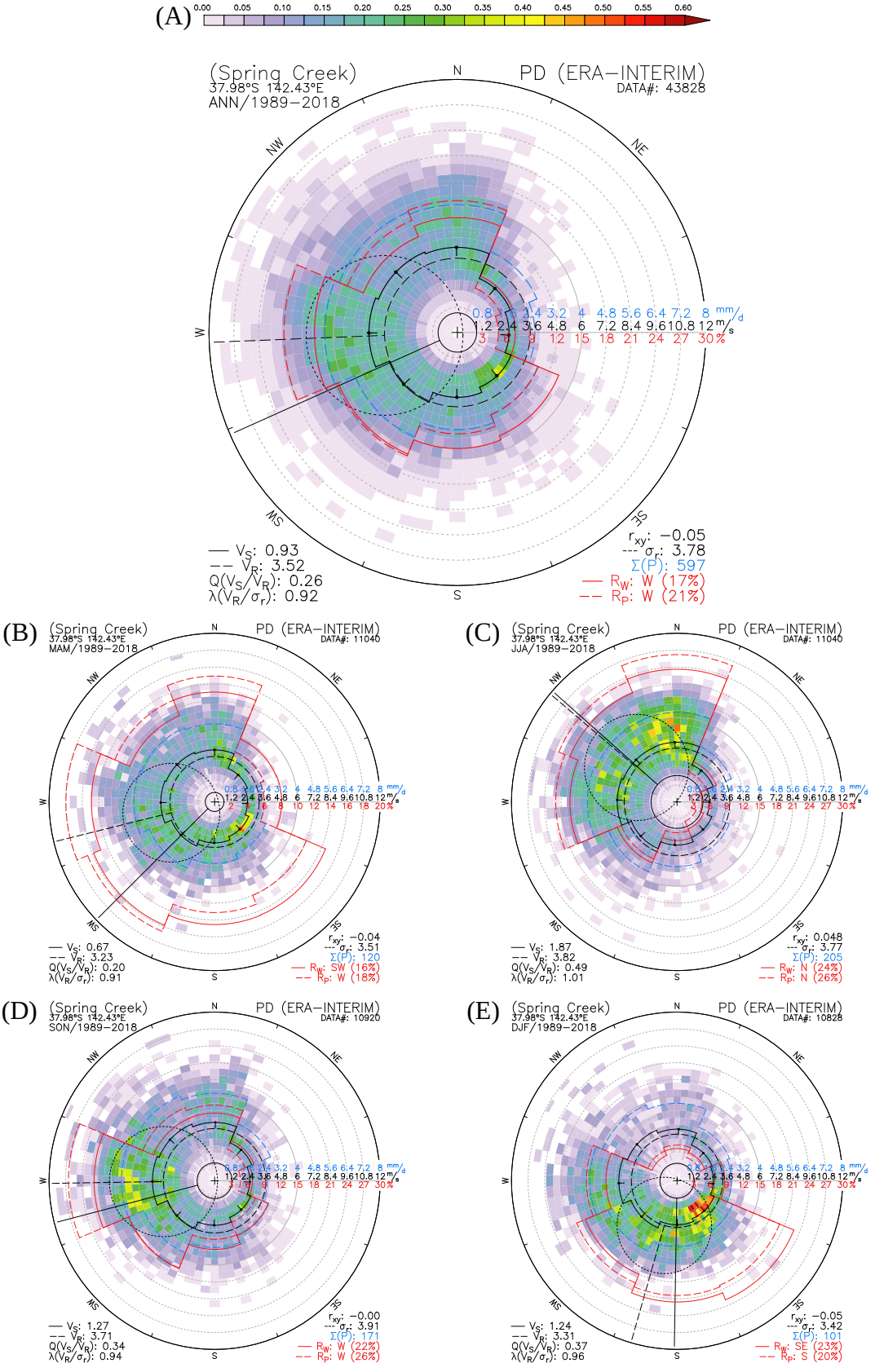

Supplementary Figure 9. Wind regime statistics for the LGM at the Willandra Lakes.

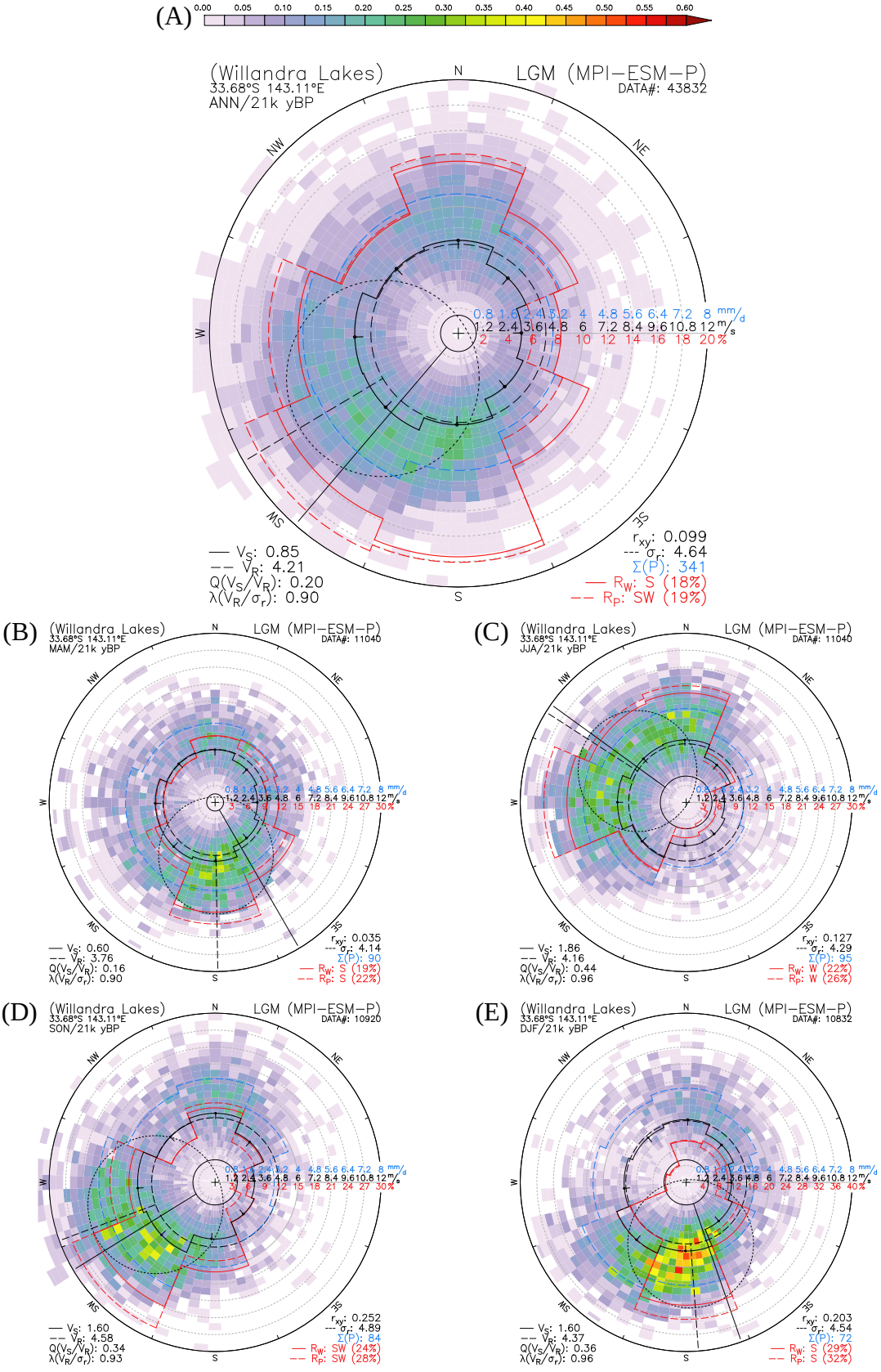

Supplementary Figure 10. Wind regime statistics for the LGM at Spring Creek.

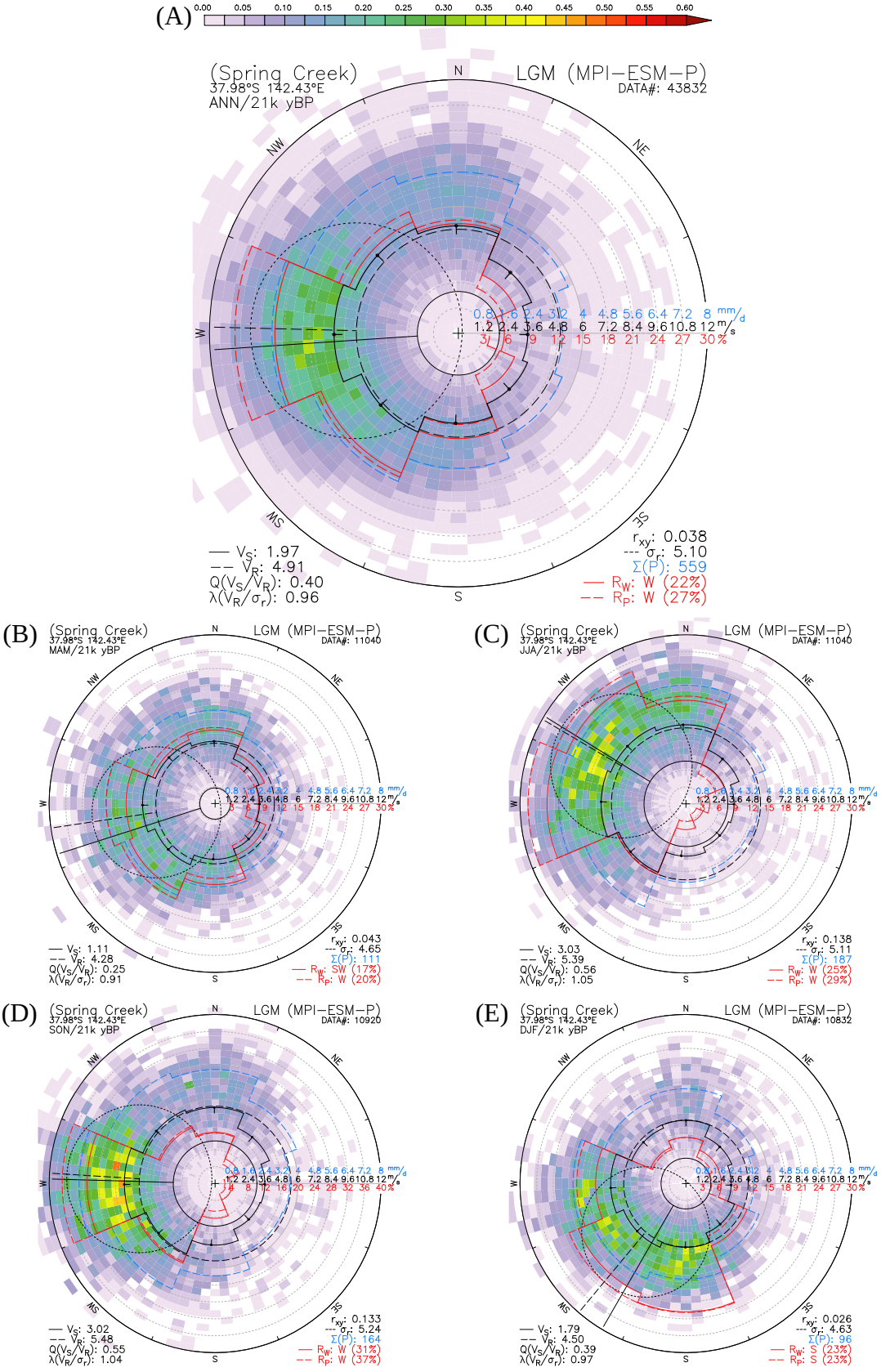

Particle transport/source footprint modelling

The following figures show results of backward trajectory modelling for particles of various sizes arriving at the Willandra Lakes and Spring Creek sites in the LGM and present-day conditions. Shaded areas present the likelihood (percent of annual total, note the non-linear scale) of a given location to act as a source for wind-mobilized dust/sand particles. Unshaded areas denote locations that were not acting as sources throughout the entire analyzed period (30 years). Note that no spatiotemporal variability of sources is assumed, in order to show the wind-triggered airmass-transport statistics only.

Figures panels present (A) Annual overall and seasonal statistics for (B) Autumn (March, April, May), (C) Winter (June, July, August), (D) Spring (September, October, November) and (E) Summer (December, January, February), respectively.

Supplementary Figure 11. Modelled source footprint for particle sizes of 20 µm arriving at the Willandra Lakes under present-day wind regimes.

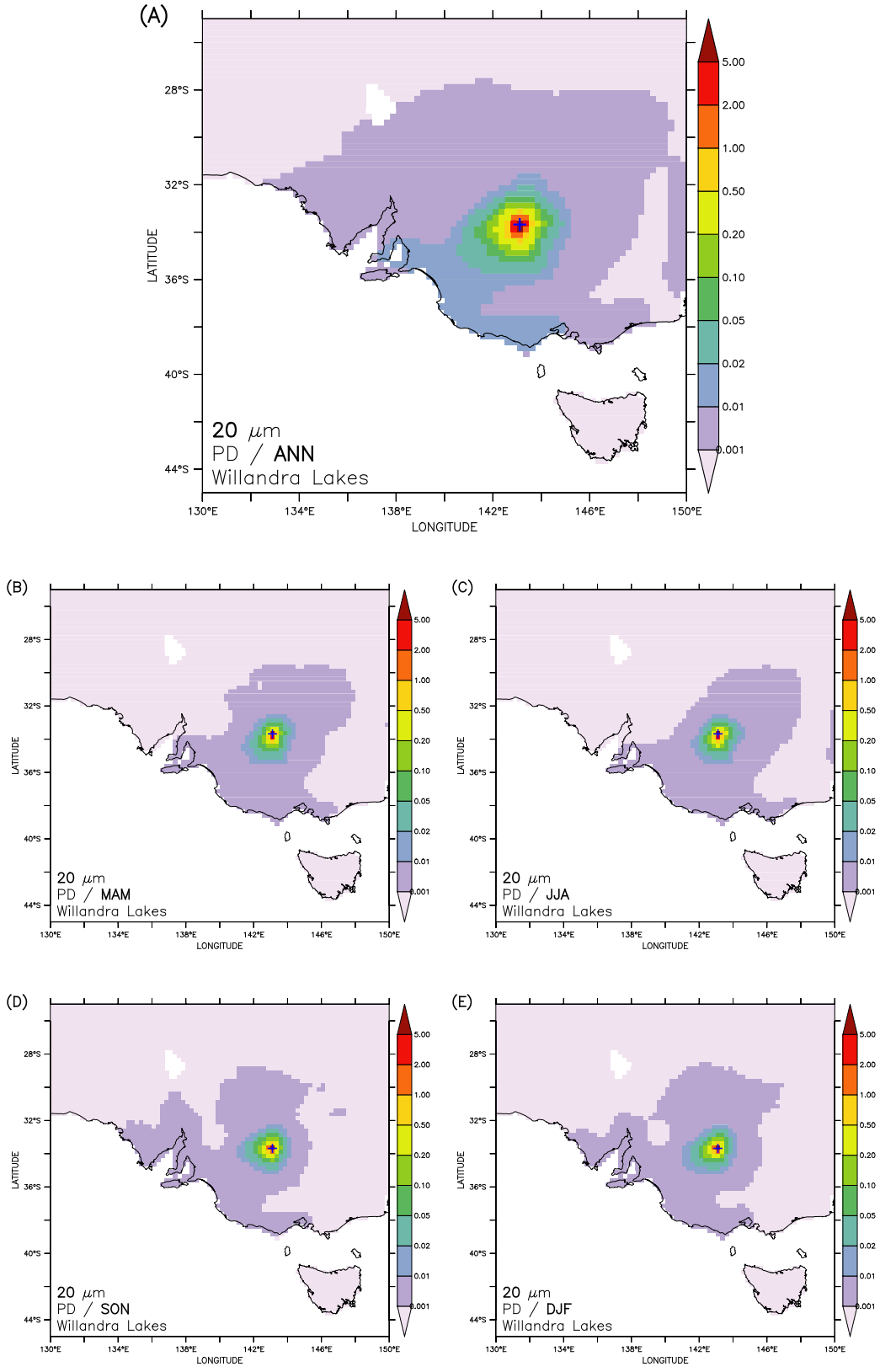

Supplementary Figure 12. Same as Supplementary Figure 11 for particle sizes of 60 µm.

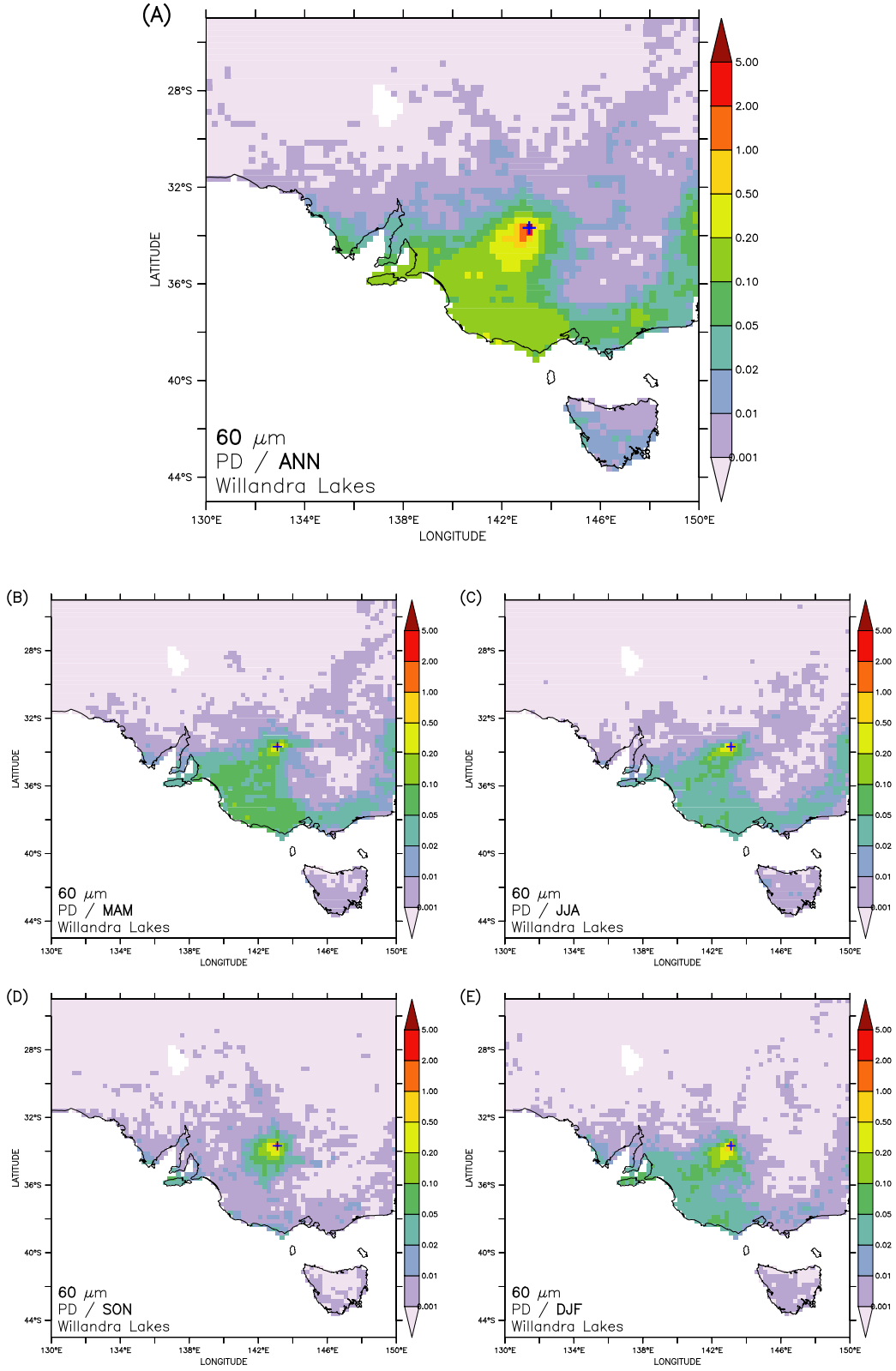

Supplementary Figure 13. Same as Supplementary Figure 11 for particle sizes of 120 µm.

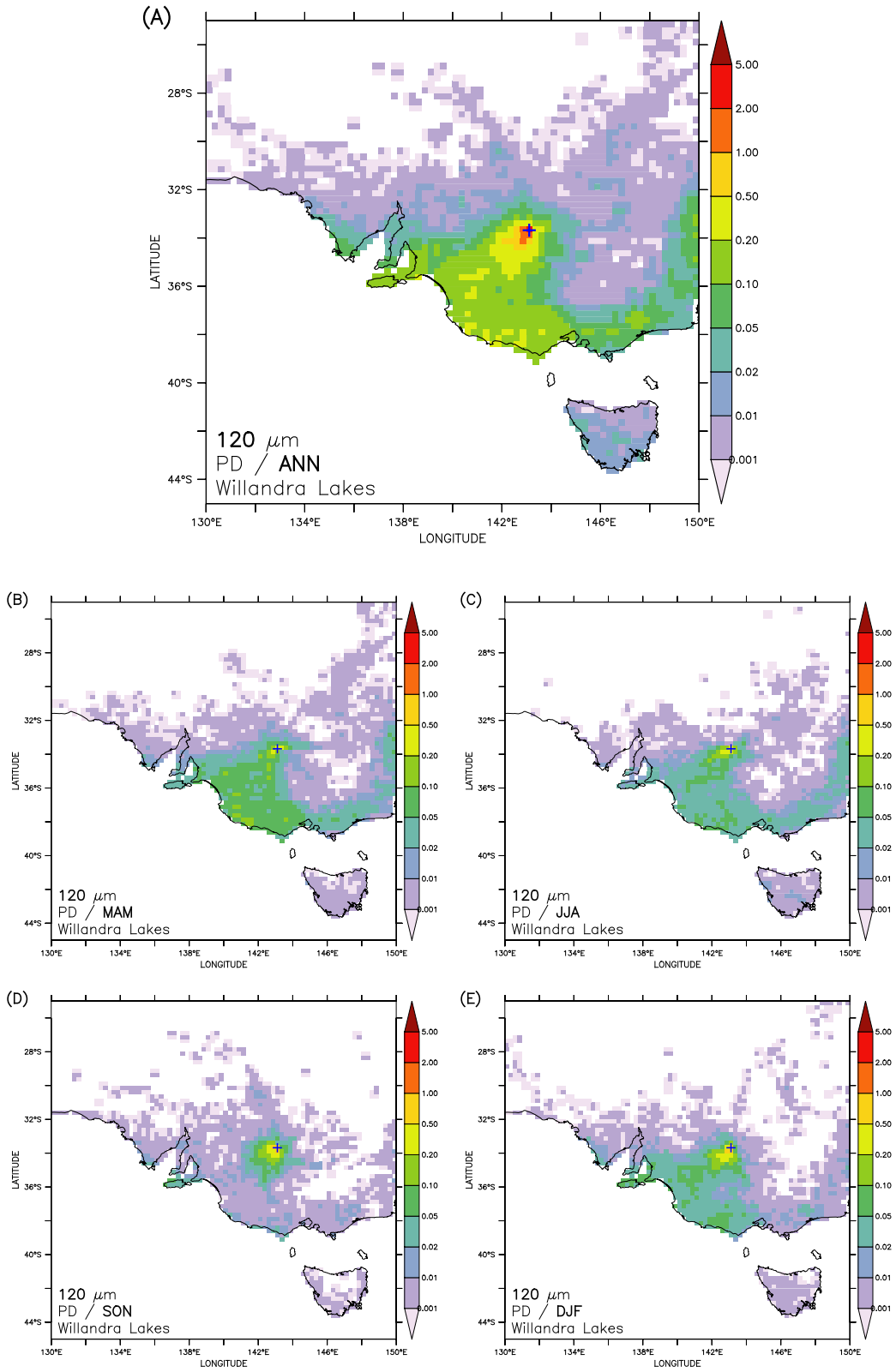

Supplementary Figure 14. Modelled source footprint for particle sizes of 20 µm arriving at Spring Creek under present-day wind regimes.

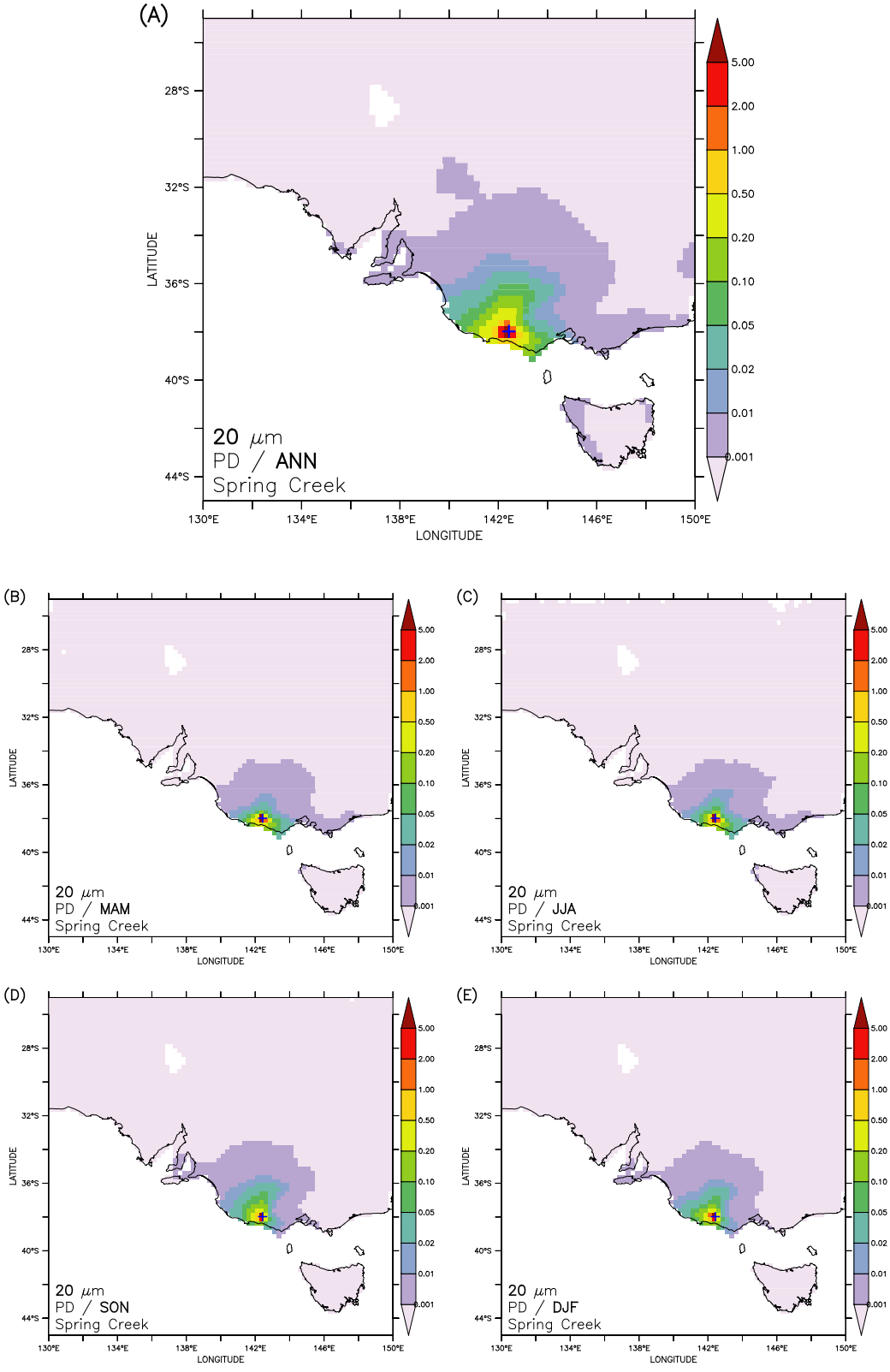

Supplementary Figure 15. Same as Supplementary Figure 14 for particle sizes of 60 µm.

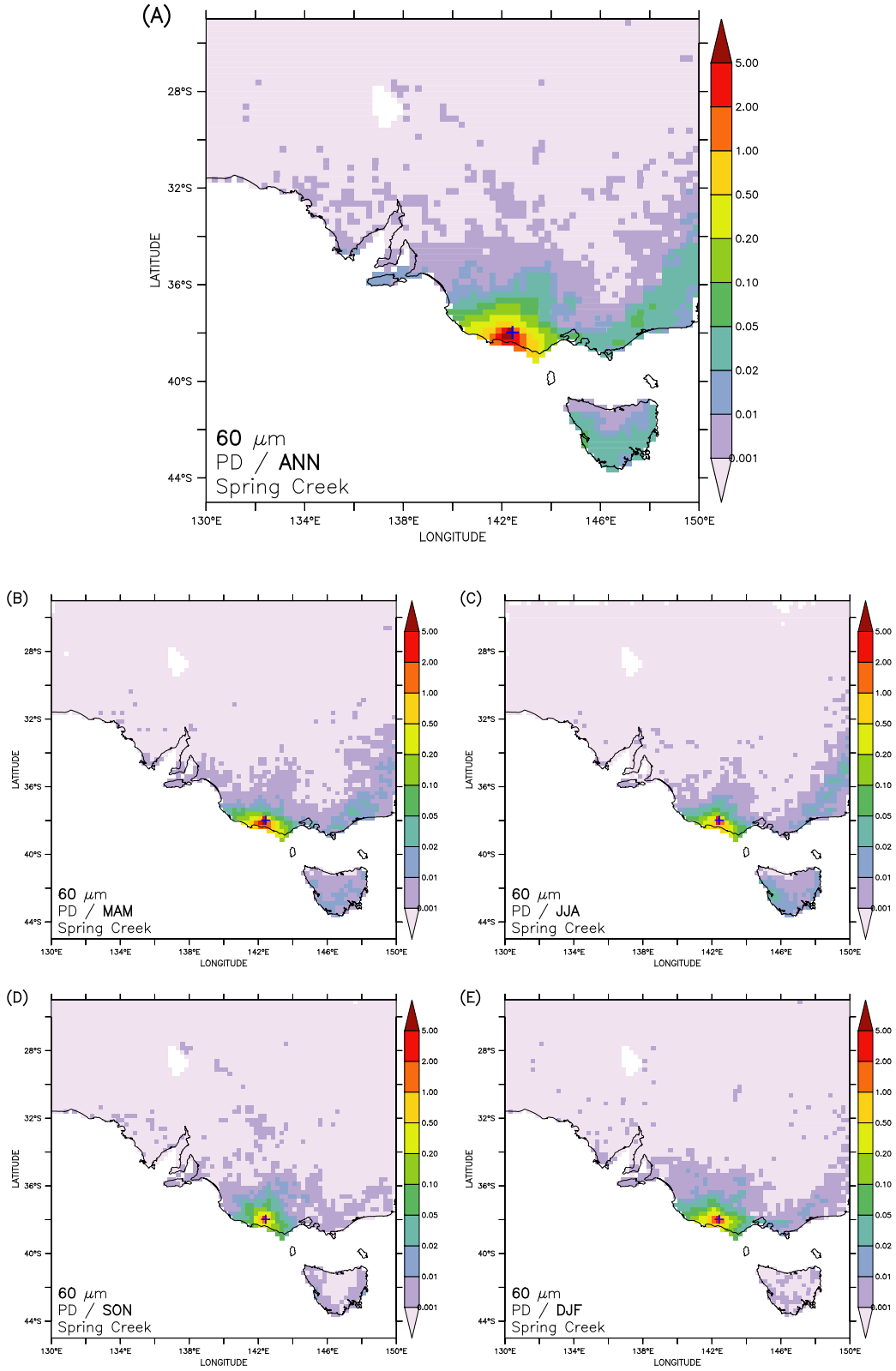

Supplementary Figure 16. Same as Supplementary Figure 14 for particle sizes of 120 µm.

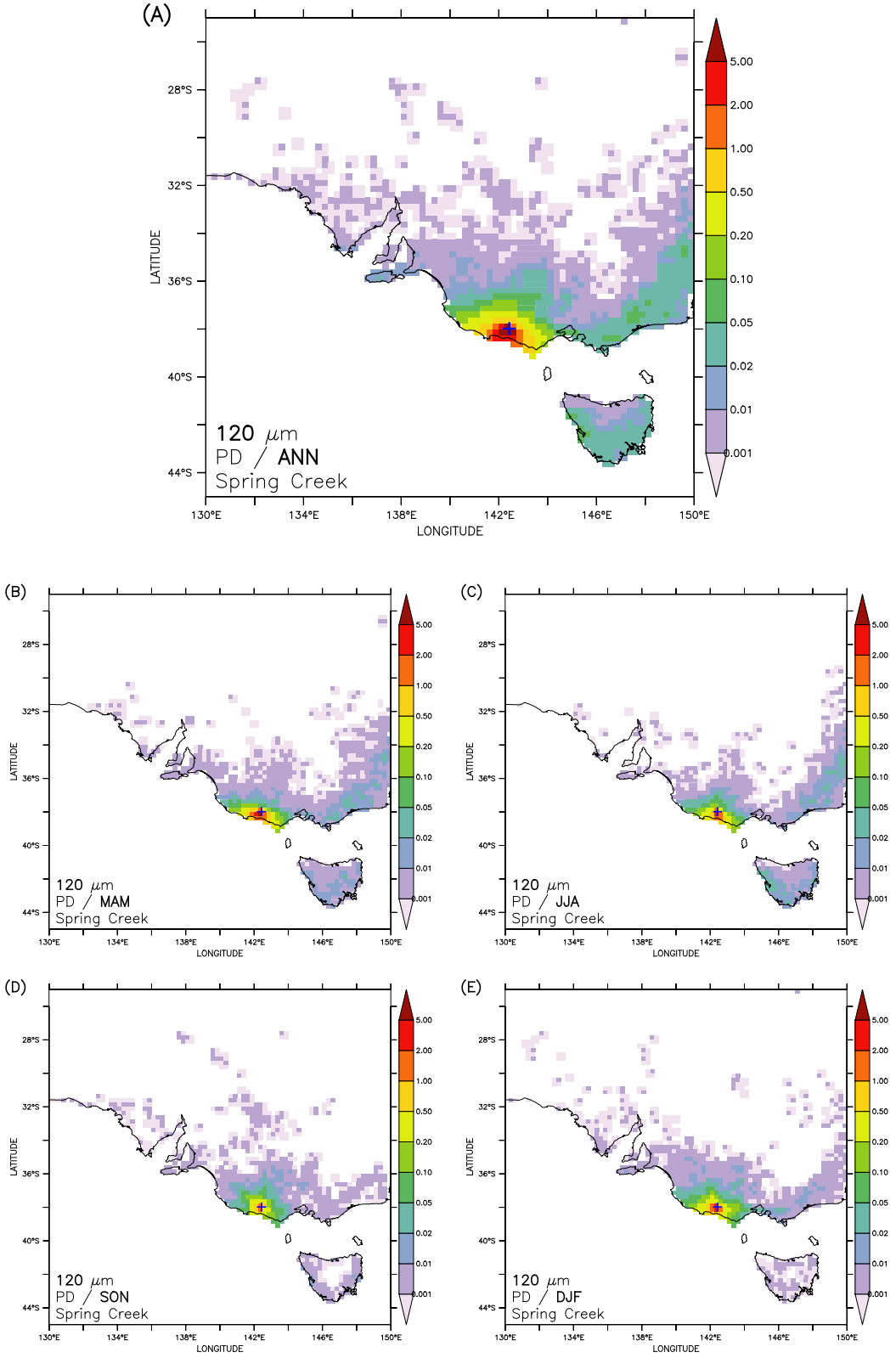

Supplementary Figure 17. Modelled source footprint for particle sizes of 20 µm arriving at the Willandra Lakes under LGM wind regimes.

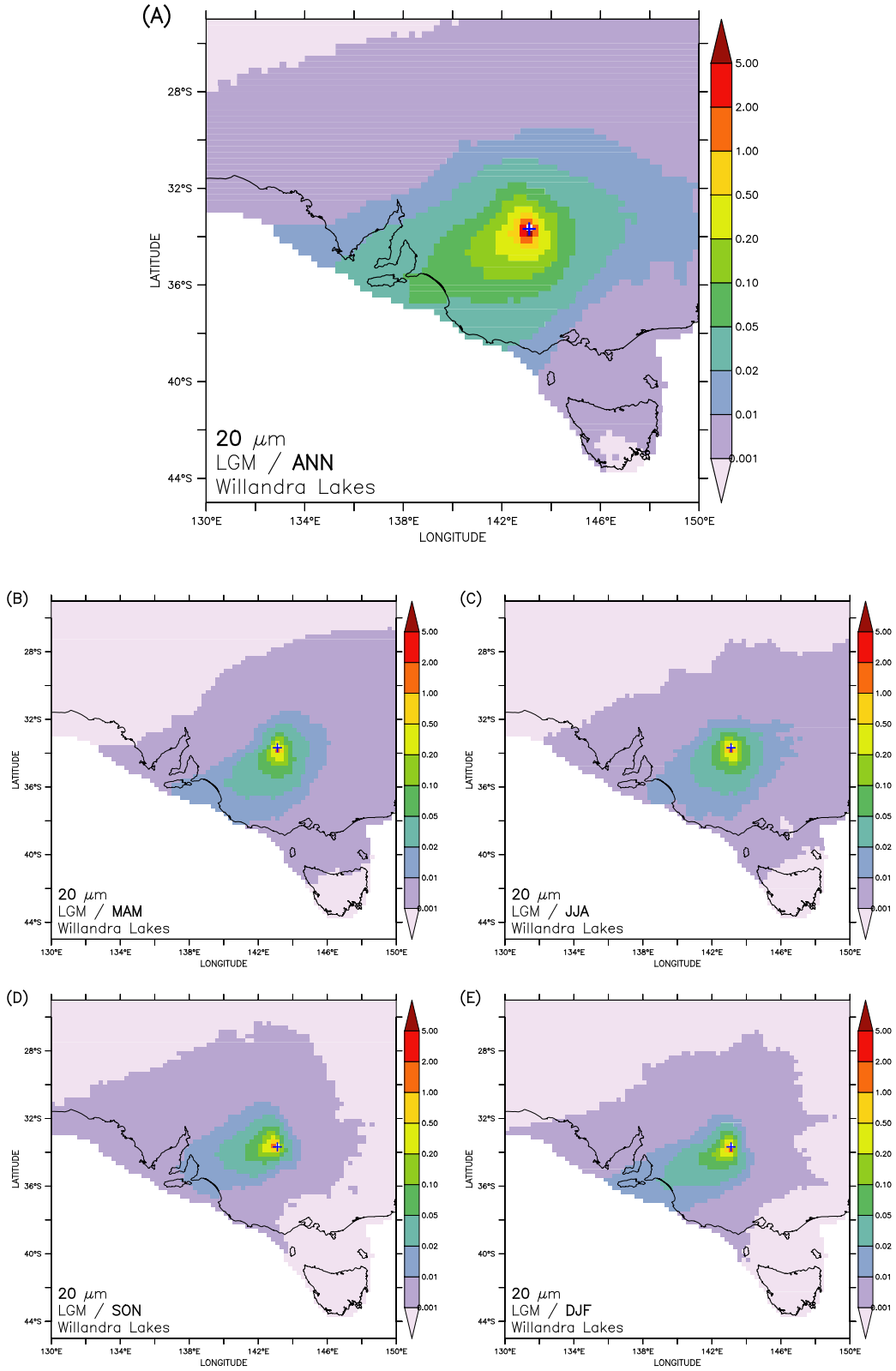

Supplementary Figure 18. Same as Supplementary Figure 17 for particle sizes of 60 µm.

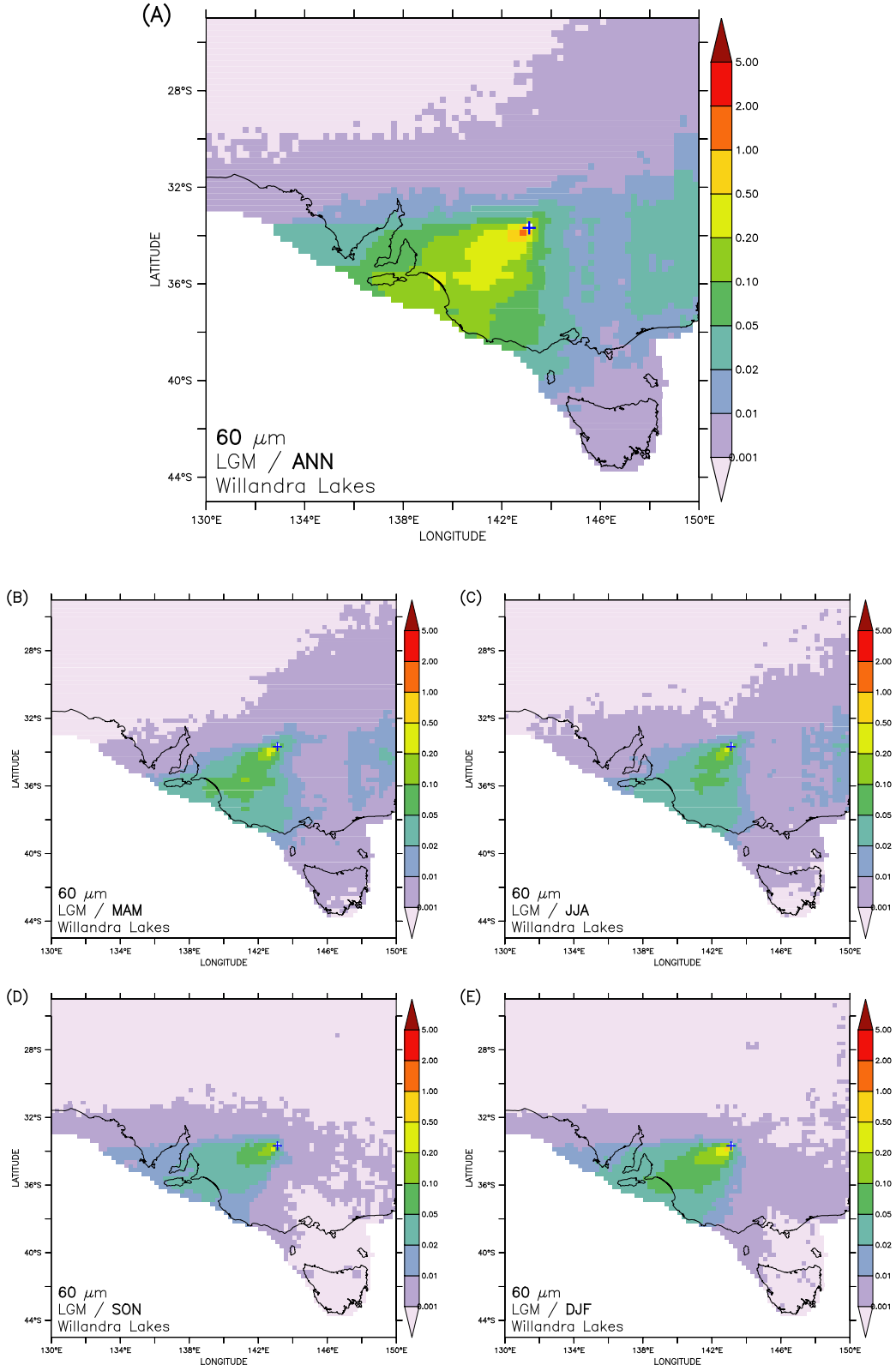

Supplementary Figure 19. Same as Supplementary Figure 18 for particle sizes of 120 µm.

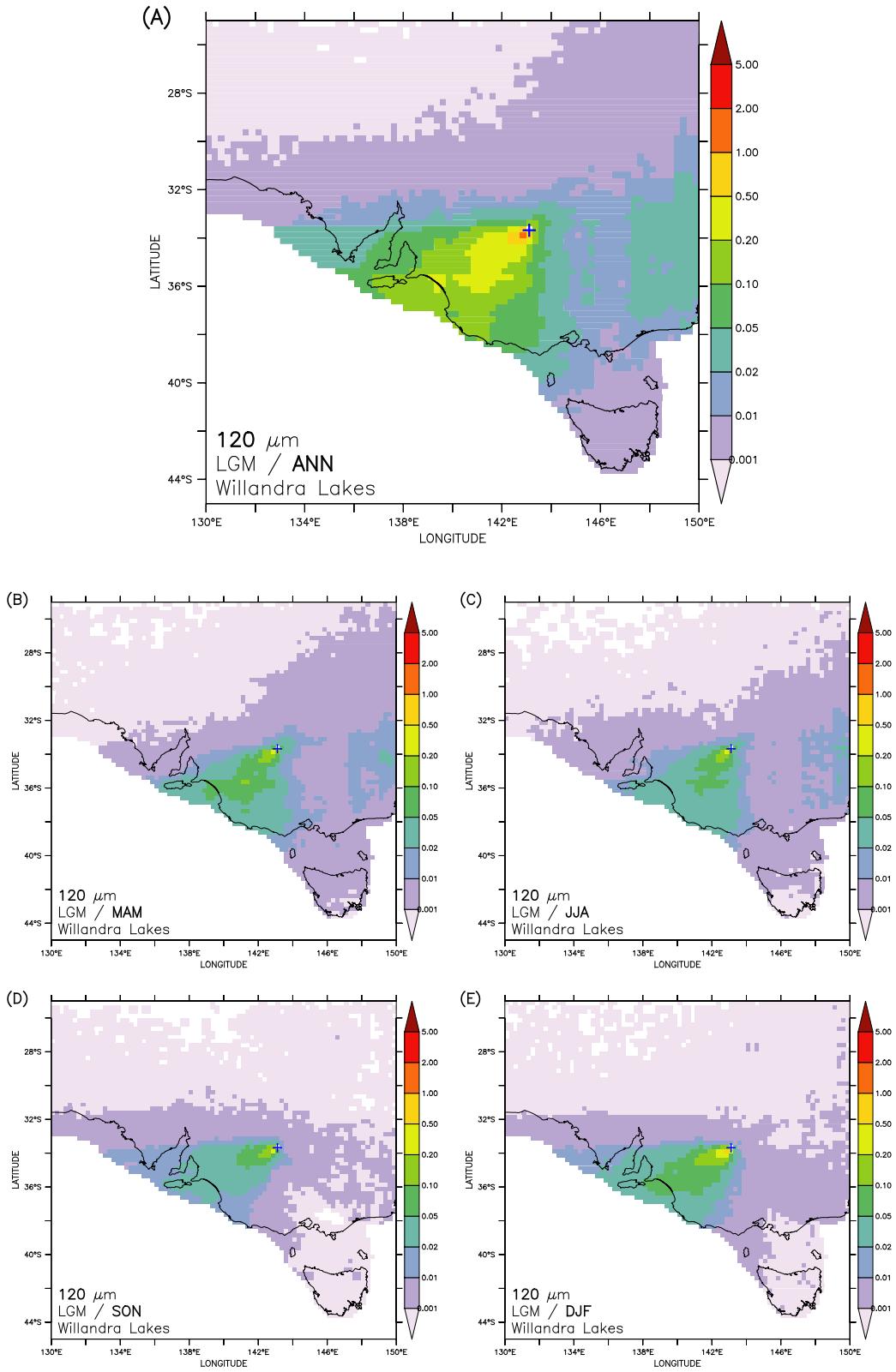

Supplementary Figure 20. Modelled source footprint for particle sizes of 20 µm arriving at Spring Creek under LGM wind regimes.

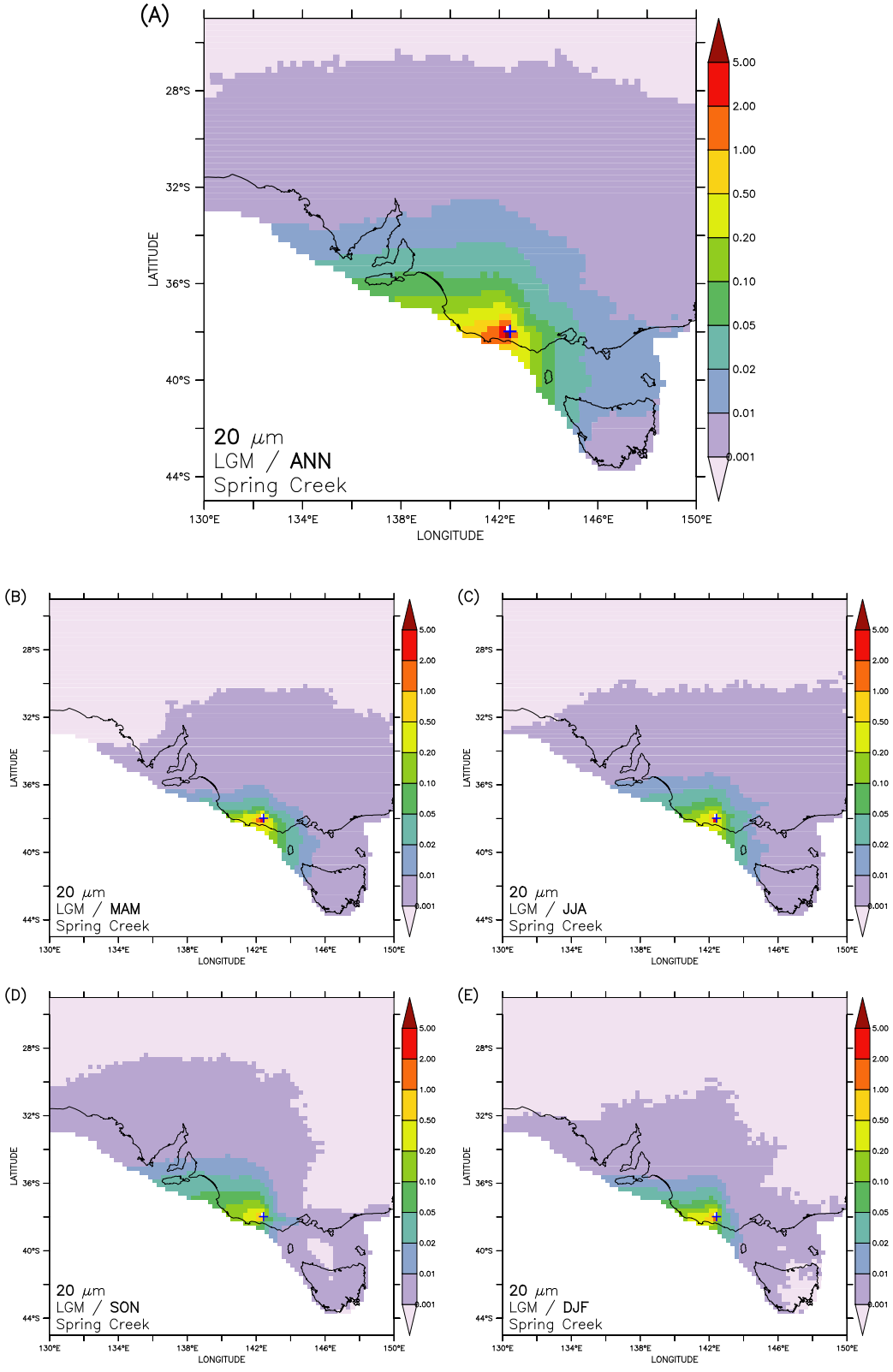

Supplementary Figure 21. Same as Supplementary Figure 20 for particle sizes of 60 µm.

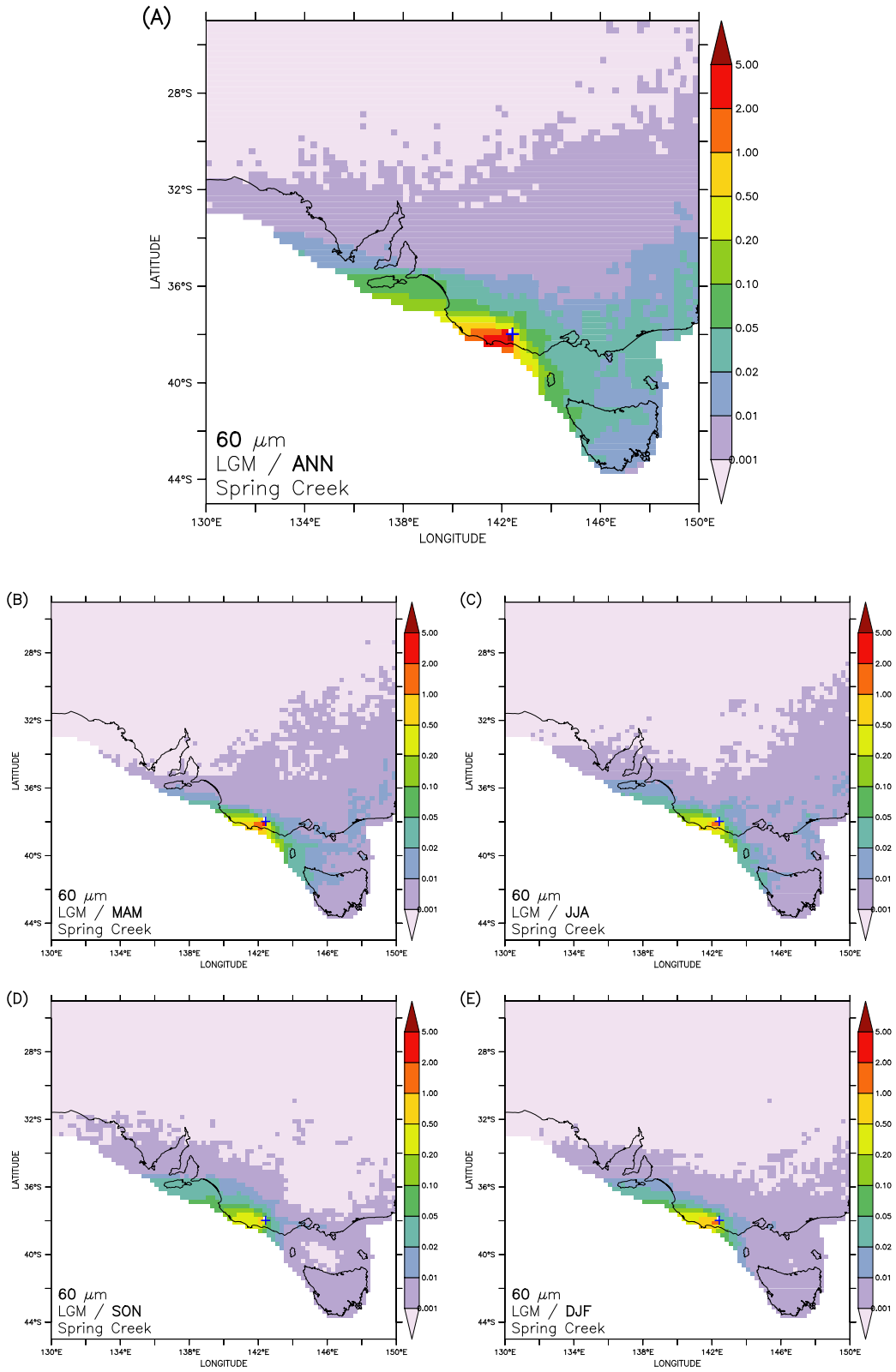

Supplementary Figure 22. Same as Supplementary Figure 20 for particle sizes of 120 µm.

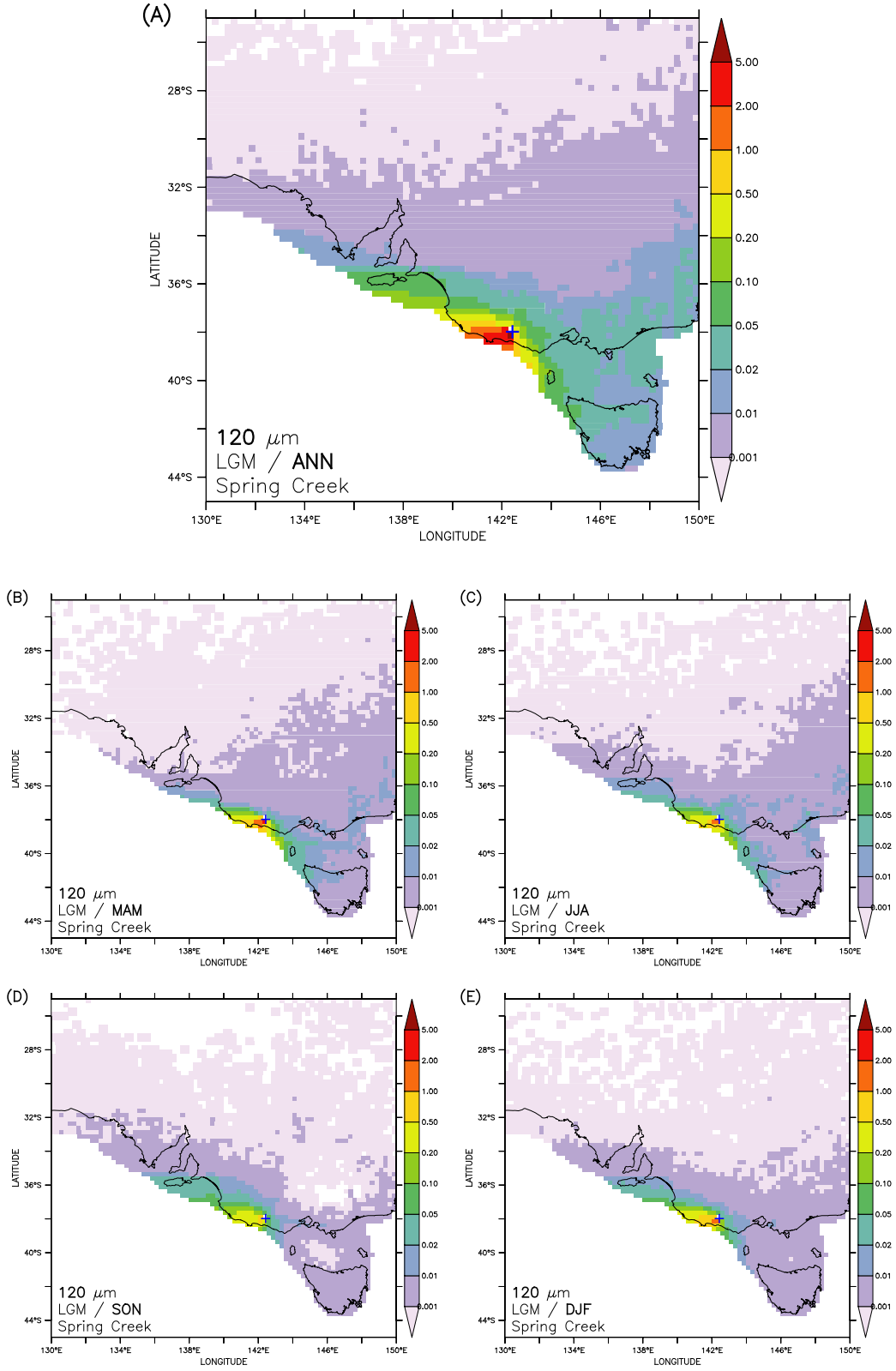

References

Adamiec, G, and M Aitken. 1998. 'Dose-rate conversion factors: update', *Ancient TL*, 16: 37-50.

Botter-Jensen, L. 1997. 'Luminescence techniques: instrumentation and methods', *Radiation Measurements*, 27: 749-68.

Botter-Jensen, L., E. Bulur, G. A. T. Duller, and A. S. Murray. 2000. 'Advances in luminescence instrument systems', *Radiation Measurements*, 32: 523-28.

Botter-Jensen, L., V. Mejdahl, and A. S. Murray. 1999. 'New light on OSL', *Quaternary Science Reviews*, 18: 303-09.

Fitzsimmons, K.E., N. Stern, C.V. Murray-Wallace, W. Truscott, and C. Pop. 2015. 'The Mungo mega-lake event, semi-arid Australia: non-linear descent into the last ice age, implications for human behavior', *PLoS One*, 10: e0127008.

Fitzsimmons, Kathryn E., Edward J. Rhodes, and Timothy T. Barrows. 2010. 'OSL dating of southeast Australian quartz: A preliminary assessment of luminescence characteristics and behaviour', *Quaternary Geochronology*, 5: 91-95.

Galbraith, R.F., R.G. Roberts, G.M. Laslett, H. Yoshida, and J. M. Olley. 1999. 'Optical dating of single and multiple grains of quartz from Jinmium rock shelter, northern Australia. Part 1, Experimental design and statistical models', *Archaeometry*, 41: 339-64.

Mejdahl, V. 1979. 'Thermoluminescence dating: beta-dose attenuation in quartz grains', *Archaeometry*, 21: 61-72.

Murray, A S, and A G Wintle. 2003. 'The single aliquot regenerative dose protocol: potential for improvements in reliability', *Radiation Measurements*, 37: 377-81.

Murray, A. S., and A. G. Wintle. 2000. 'Luminescence dating of quartz using an improved single-aliquot regenerative-dose protocol', *Radiation Measurements*, 32: 57-73.

Porch, Nick, and A. Peter Kershaw. 2010. 'Comparative AMS 14C dating of plant macrofossils, beetles and pollen preparations from two late Pleistocene sites in southeastern Australia.' in S. Haberle, J. Stevenson and M. Prebble (eds.), *Altered Ecologies (Terra Australis 32): Fire, climate and human influence on terrestrial landscapes* (Australian National University EPress: Canberra).

Prescott, J. R., and J. T. Hutton. 1994. 'Cosmic ray contributions to dose rates for luminescence and ESR dating: Large depths and long term variations', *Radiation Measurements*, 23: 497-500.

White, J. Peter, and Tim Flannery. 1995. 'Late Pleistocene Fauna at Spring Creek, Victoria: A Re-Evaluation', *Australian Archaeology*, 40: 13-17.